Journal of Environmental Management 247 (2019) 356–362

Contents lists available at ScienceDirect

Journal of Environmental Management

journal homepage: www.elsevier.com/locate/jenvman

Research article

A facile polymerisation of magnetic coal to enhanced phosphate removal from solution

George William Kajjumba[a,*], Eren Yıldırım[b], Serdar Aydın[c], Serkan Emik[b], Tuba Ağun[c], Faisal Osra[d], Joseph Wasswa[e]

[a] Department of Civil and Environmental Engineering, University of Nevada, LV, USA
[b] Department of Chemical Engineering, Istanbul University-Cerrahpaşa, Istanbul, Turkey
[c] Department of Environmental Engineering, Istanbul University-Cerrahpaşa, Istanbul, Turkey
[d] Department of Civil Engineering, Umm Al-qura University, Makkah, Saudi Arabia
[e] Department of Civil and Environmental Engineering Syracuse University, NY, USA

ARTICLE INFO

Keywords:
Wastewater quality
Adsorption kinetics
Carbon
Phosphorus removal
Conducting polymer
Emerging contaminants

ABSTRACT

Globally, there are increased threats to available freshwater resources due to pollution, climate change, and increased demand from population growth. Phosphorus is one of the essential nutrients required for animal and plant growth. However, when it is released into freshwater resources in excess amounts, it can become a pollutant through eutrophication. This study aimed to enhance the removal of phosphate from water using modified coal. The coal was magnetised by *in-situ* synthesis using a precipitation technique. To obtain functional groups and mechanical stability, magnetised coal particles were coated with polyaniline, via the polymerisation of aniline to form Magnetised Unburnt Coal Polyaniline (MUC-PANI). The properties of MUC-PANI were investigated using TGA, BET, XRD, Raman spectroscopy, SEM, and FTIR. TGA reviewed MUC-PANI as 58% magnetised coal and 42% polyaniline, while the specific surface area increased from 30.0 to 42.2 m^2/g after modification. SEM indicated a cauliflower structure on the surface of MUC-PANI due to the successful polymerisation of polyaniline. The FTIR spectrum showed successful adsorption of phosphate due to the formation of incipient peak at1008 cm^{-1}. The adsorption kinetic data are better fitted to the Elovich model. The Langmuir adsorption capacity of MUC-PANI is 147.1 mg PO_4^{3-}/g at 25 °C and pH 5.0 (initial concentration 10-200 mg/L, dose 0.8 g/L). MUC-PANI is a cost-efficient compound for removal of phosphate because it is made from readily available coal.

1. Introduction

Phosphorus is a crucial limiting nutrient for primary production in ecosystems and an essential element in cellular composition. However, the presence of phosphorus (above 1.0 mg/L) in water bodies causes eutrophication The main sources of excess phosphorus in water are industrial and agricultural runoff; thus, the removal of phosphorus from wastewater, before it is discharged into water bodies is a necessity. In developing economies, phosphorus levels are increasing at alarming rates due to the increased utilisation of phosphorus infused products (e.g. pigments), as well as limited advanced wastewater treatment technologies (Cai et al., 2013; Hao et al., 2018).

Different techniques have been developed to remove phosphorus from solutions, including chemical precipitation (Darwish et al., 2017), adsorption (Mo et al., 2018; Wang et al., 2018; Wu et al., 2019), and biological methods (Hao et al., 2018; Mujtaba et al., 2017). The latter being the most commonly applied because of its ability to remove ammonia, phosphorus and biological oxygen demand simultaneously. However, pH, temperature, residence time, and organic loading affect the biological process. Therefore, to achieve strict effluent phosphorus concentration levels, biological approaches need reinforcement with additional methods.

Adsorption is one of the most common methods applied in water and wastewater treatment. Different adsorbents have been evaluated by various research groups for the removal of phosphate from water (Su et al., 2013; Yang et al., 2018). The suitability of any adsorbent is governed by its adsorption capacity, availability, and cost. Carbon-related adsorbents have received considerable attention in the treatment of wastewater; however, the use of coal as an adsorbent is still limited. Coal consumption is expected to decrease due to growing advocacy and

* Corresponding author. 4505 S Maryland Pkwy, Las Vegas, NV, 89154, USA.
E-mail address: gwkajjumba@gmail.com (G.W. Kajjumba).

https://doi.org/10.1016/j.jenvman.2019.06.088
Received 3 February 2019; Received in revised form 15 June 2019; Accepted 17 June 2019

reliance on green energy. Unburnt coal contains a significant amount of carbon (Gupta, 2018) that can be exploited in several ways. Therefore, with the projected reduction of coal utilisation as an energy source, alternative, environmentally friendly use should be assessed.

Coal waste has been successfully applied in the removal of vanadium from solution; however, rapid separation of the adsorbent from the solution, after adsorption, presented a challenge (Kajjumba et al., 2018a). It can be hypothesised that the impregnation of magnetic elements (iron, nickel, neodymium) could ease the parting of the adsorbent upon the application of an external magnet. Additionally, the coating of conducting polymers (polyacetylene, polypyrrole, polyaniline) on magnetic coal could improve the mechanical stability, specific surface area, and adsorption capacity. Therefore, the objectives of this study were to (i) synthesize an efficient adsorbent from coal, using conducting polymers; (ii) compare the phosphate adsorption performances under various reaction times, initial phosphate concentrations, temperatures, and pH values; (iii) elucidate probable adsorption mechanisms and characterizations using Fourier transform infrared (FTIR) spectrometer, X-ray diffraction (XRD), and zeta potential.

2. Materials and methods

2.1. Chemicals

The coal used in this study was mined from Trakya (GPS: 41.141968N, 28.353888E). Iron (III) chloride ($FeCl_3.6H_2O$, 98-102%), iron (II) chloride ($FeCl_2.4H_2O$, 99%), and ammonium hydroxide (NH_4OH, 26%) were used in the synthesis of magnetic particles. Aniline ($C_6H_5NH_2$), ammonium persulfate ($(NH_4)_2S_2O_8$, 98%) and hydrochloric acid (HCl, 37%) were used to generate polyaniline structures. Sodium dihydrogen phosphate anhydrous (NaH_2PO_4) was expended to prepare a standard phosphate solution, while sodium hydroxide (NaOH, 99%) and HCl were expended on altering the pH, and during the regeneration process. Merck supplied all of the chemicals. Deionised water (conductivity 0.15 µS/cm) was used in all of the experiments.

2.2. Magnetic unburnt coal synthesis

Coal was cleaned with deionised water and then dried for 36 h at 110 °C. The dried material was then conditioned using 1M NaCl for 24 h to improve the dissolution of silica compounds to the amorphous structure. It was then sieved and washed again with deionised water and dried at 110 °C for 36 h. To produce magnetic coal, 75 ml of 0.15M $FeCl_2.4H_20$ (1.71 g) and 150 ml of 0.15M $FeCl_3.6H_2O$ (3.65 g) were mixed with 3 g of coal for 30 min at 80 °C, in a three neck reactor, under a nitrogen atmosphere; afterwards, 50 ml of 2M NH_4OH were added rapidly to adjust the pH to around 10, as seen in Eq. (1) and Fig. 1a (Mthombeni et al., 2016). The temperature of the resultant mixture was maintained at 80 °C and 400 rpm for 1 h. The formed magnetic coal was collected by an external magnet, cleaned with deionised water, and dried under a vacuum for 24 h at 40 °C.

$$Fe^{2+} + 2Fe^{3+} + 8OH^- \underset{pH\ 10}{\rightarrow} Fe_3O_4 + 4H_2O \quad (1)$$

2.3. Magnetic unburnt coal polyaniline (MUC-PANI) synthesis

To synthesise MUC-PANI, 2.7 ml of aniline solution was mixed with 50 ml of 0.1M HCl (200 rpm) for 20 min at a temperature near 0 °C; then 3.0 g of magnetised coal was added and stirred vigorously for 10 min. For polymerisation, 8.55 g of $(NH_4)_2S_2O_8$ were mixed with 50 ml of 0.1M HCl, then added slowly; the resultant mixture was stirred for 5 h, as seen in Fig. 1b. To the resultant mixture, 50 ml of 1M NH_4OH was added (to neutralise), and the system was left to age for 36 h (Yang et al., 2005). The possible chemical interactions are represented in the following equation (2):

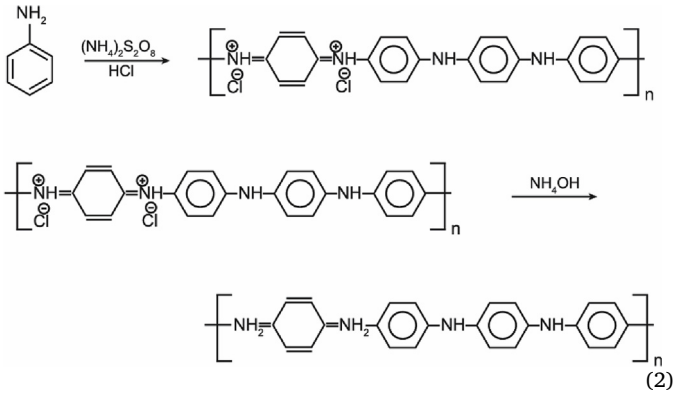

(2)

The solution was filtered with the help of an external magnet, and the formed MUC-PANI was washed with methanol to remove oligomers and non-polymeric impurities. Then the MUC-PANI was washed with deionised water until a neutral pH was attained, and dried under a vacuum for 24 h at 40 °C; 4.4 g of MUC-PANI were synthesised.

2.4. Characterisation

A Spectrum One PerkinElmer (USA) model FTIR spectrometer was used to study the chemical characterisation of MUC-PANI before and after adsorption. A Thermo-gravimetric Analyser (TGA) (model: LINSEIS STA PT1750) was used to analyse the thermal behaviour, as well as the amount of magnetic material and polyaniline formed on the coal. While Raman spectroscopy (PerkinElmer Raman) was used to clarify Fe_2O_3 hexagonal and Fe_3O_4 polyhedral particles. X-ray Diffraction, (XRD) (Rigaku smart-Lab model) and Scanning Electron Microscopy (SEM) (model JEOL/JSM-6610) were used to study the morphology of the coal. The specific surface characteristics were assessed with a Quantachrome Autosorb Brunauer-Emmett-Teller (BET) equipped with a gas sorption analyser. The zeta potential was measured using a Zetasizer Nano–ZS90 Instrument, Malvern, at 25 °C.

2.5. Batch adsorption studies

The standard phosphate solution was prepared by dissolving NaH2PO4 in deionised water. Adsorption batch studies were assessed by agitating 0.8 g/L of the MUC-PANI with 20 ml of a phosphate solution (10-200 mg/L) for at least 5 h at 140 rpm. The pH effect was studied by changing the pH from 2.0 to 11 by adding dilute HCl and NaOH solutions. The competition between phosphate and other anions was analysed using Na_2CO_3, Na_2SO_4, and $NaNO_3$. After adsorption, the solution was filtered through a 0.45 µm filter before it was analysed with Ion Chromatography (model: ICS-1100) to determine the residual phosphate. The equilibrium amount of phosphate adsorbed was determined using Eq. S(1).

2.6. Regeneration of MUC-PANI

For economic purposes, regeneration is necessary to examine the reusability of an adsorbent. Low reusability generally means high production and operating costs, which can make the application of the adsorbent impractical even though it may have a high adsorption capacity. Used MUC-PANI was mixed with 50 ml of 1M NaOH for 24 h at 25 °C to desorb the phosphate. The desorbed MUC-PANI was put in contact with 2M HCl for 3.0 h for regeneration, dried at 110 °C, and reused (Mthombeni et al., 2016).

2.7. Statistical analysis

Adsorption experiments were conducted in triplicates; statistical analysis was performed using Microsoft Excel 2013 and OriginPro 8.0

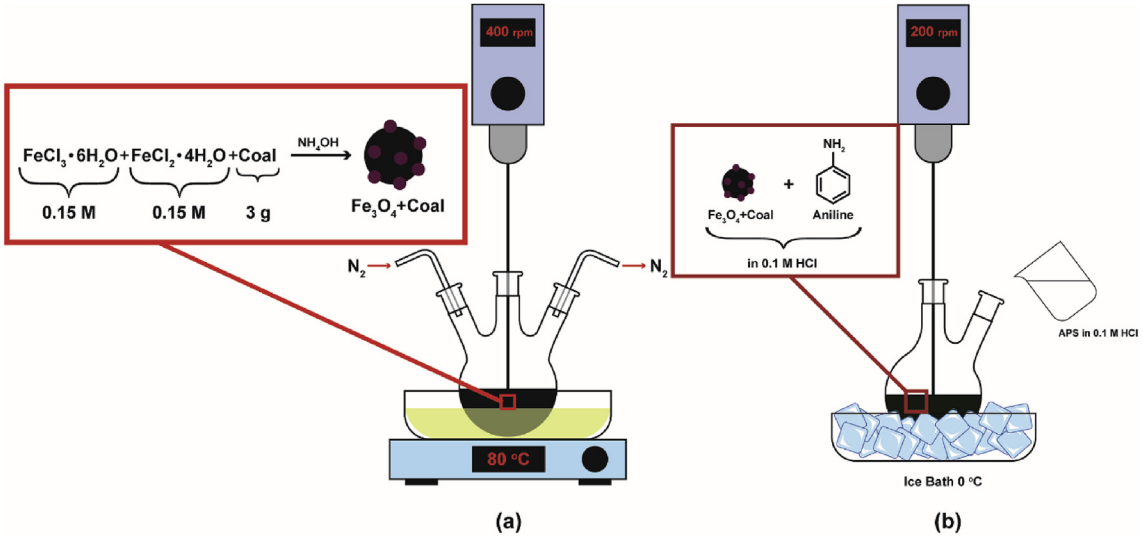

Fig. 1. Preparation of (a) magnetic unburnt coal, (b) magnetic unburnt coal-polyaniline.

(OriginLab Corporation, Northampton, MA). Experimental results were expressed as mean. The values in the figures were presented with standard error deviation.

3. Results and discussion

3.1. Characterisation of the adsorbent and adsorption mechanism

Table 1 shows the physiochemical properties of the coal and MUC-PANI, while Table S3 shows the corresponding chemical compositions. The coal was composed mainly of carbon, silicon, and aluminium. Compared to the raw coal, the contents of iron, nitrogen, and carbon increased, while the loss on ignition of the MUC-PANI increased after the introduction of polyaniline. The analysis of the magnetised unburnt coal (MUC) with TGA data indicated that 25% of the composite was magnetic and 75% coal, while the MUC-PANI composition was 58% MUC, and 42% PANI (Section S3.1). Fig. S4 shows the TGA curves of the unburnt coal, magnetised coal, and MUC-PANI. All curves show minor weight loss at 100 °C, which is attributed to the loss of free moisture. The weight loss between 100 °C and 260 °C is due to the removal of volatile compounds. The weight loss between 260 °C and 700 °C is ascribed to the degradation of carbon moieties that form the coal, while above 700 °C is attributed to the dihydroxylation of muscovite (Földvári, 2011).

The XRD pattern of the coal (Fig. 2a and Table S3) shows a typical characteristic of coal with a diffraction peak at $2\theta = 12.45^0$ associated with the kaolinite and inter-planar spacing of 0.711 nm. At $2\theta = 26.6^0$, a significant peak is induced by quartz, with a d-spacing of 0.669 nm (Chindaprasirt et al., 2009; Yuan et al., 2016). The small peak at $2\theta = 35^0$ corresponds to goethite; other peaks correspond to illite, muscovite, and gibbsite (Liu et al., 2012). Upon modification, the peak of goethite increased (Fig. 2b), showing the penetration of more ironic materials. After polymerisation, at low diffraction angles the intensity

Table 1
BET properties of coal and MUC-PANI.

Parameter	Coal	MUC-PANI
Particle size (mm)	0.250–0.650[a]	< 0.250[a]
Specific surface area (m^2/g)	30.00	42.20
Total pore volume (cm^3/g)	0.0488	0.210
Average pore diameter (Å)	32.58	103.8

[a] Measured with Zetasizer Nano–ZS90.

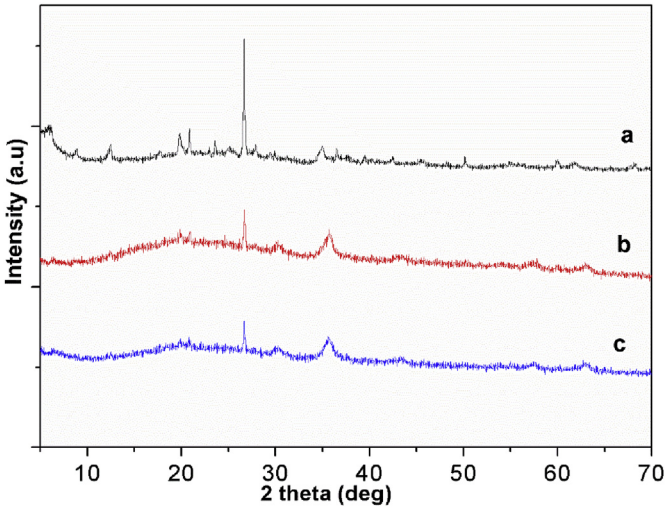

Fig. 2. XRD patterns for (a) Coal, (b) MUC-PANI, and (c) used MUC-PANI.

of the peaks decreased, showing a change from crystalline to amorphous structure. The amorphous structure is more efficient during adsorption than a crystalline structure (Yang et al., 2018). The change to an amorphous phase suggests the attachment of polyaniline on the surface of the coal; thus, MUC-PANI was successfully synthesised. Comparing the XRD pattern before (Fig. 2b) and after adsorption (Fig. 2c), there is minimal change in the diffractions; therefore, the formed MUC-PANI is a stable adsorbent.

The characteristic reflections in the Fe_3O_4 phase and the Fe_2O_3 phase are about the same. To clarify the phase of polyhedral particles, the Raman spectroscopy of MUC-PANI and Fe_3O_4 polyhedral particles was conducted. α-Fe_2O_3 can be characterised by four strong peaks at 225, 299, 412, and 613 cm^{-1}, while Fe_3O_4 is characterised by peaks at 538 and 668 cm^{-1} (Lu and Tsai, 2014). The appearance of a peak at 670 cm^{-1}, Fig. S5 shows the presence of Fe_3O_4 polyhedral particles in coal.

Unburnt coal shows a smooth surface with regular aggregated particles (Fig. S6). A close assessment of the SEM image (Fig. 3a) shows that the polyaniline formed a spiral network around the magnetised coal. The comparison of SEM images taken before and after adsorption (Fig. 3b) shows no major change in the morphology of the adsorbent; thus, MUC-PANI is a mechanically stable adsorbent.

Table 1 shows the BET results: specific surface area, pore diameter,

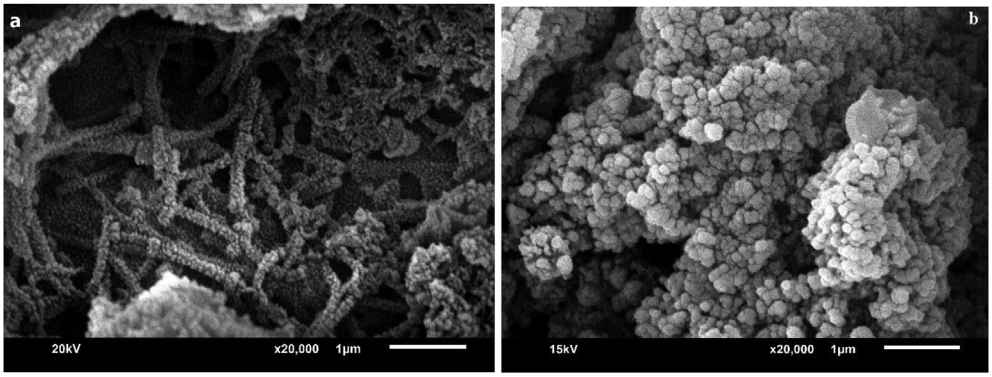

Fig. 3. SEM images of MUC-PANI (a) before and (b) after adsorption.

and total pore volume. The BET surface area and pore volume of MUC-PANI were higher than those of coal, which is due to the modification. The average pore diameter of the coal was 32.58 Å, which improved the penetration of the magnetic material to the inner region of the coal, increasing the pore diameter to 103.83 Å.

Fig. 4a shows the FTIR spectrum of the coal. After the *in-situ* synthesis of Fe_3O_4 in the coal matrix, the O-H band at 3386 cm^{-1} (Li et al., 2010) was almost lost, indicating a chemical reaction occurred during the synthesis, Fig. 4b. The formation of a 626 cm^{-1} peak, the shift of a 512 cm^{-1} peak to 521, and the coal's reduction in intensity indicate the formation of Fe_3O_4 in the matrix (Mthombeni et al., 2016). After the polymerisation of polyaniline (emeraldine) (Fig. 4c), the FTIR characteristic peaks of the MUC-PANI were close to those of polyaniline (Hallajiqomi and Eisazadeh, 2017); thus, polyaniline was successfully formed on the surface of the MUC-PANI composite.

The MUC-PANI spectrum shows incipient peaks at 1563, 1487, 1305, and 810 cm^{-1}. These peaks correspond to a C=C stretching vibration of the quinoid ring, a C=C stretching vibration of the benzenoid ring, a C-N stretching vibration, a C-H in-plane deformation, and a C-H out-of-plane deformation, respectively (Socrates, 2004). After adsorption (Fig. 4d), there is a formation of a weak band at 1008 cm^{-1}; this peak is a result of phosphate adsorption (Socrates, 2004; Xie et al., 2014) on the MUC-PANI. Comparing Fig. 4c and d, the shift, weakening, disappearance, and formation of new peaks show the adsorption of phosphate in the MUC-PANI matrix. This formation of a second network on the MUC-PANI indicates that the adsorption of phosphate may be chemisorption in nature (Emik, 2014) through ligand and/or ion exchange.

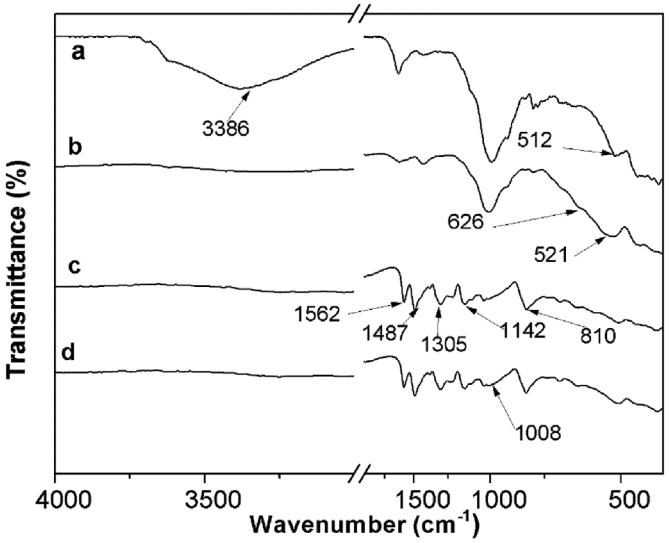

Fig. 4. FTIR spectrum of (a) coal, (b) MUC, (c) MUC-PANI before adsorption, and (d) MUC-PANI after adsorption.

3.2. pH effect

pH is an important parameter that determines the interaction between the adsorbent and the adsorbate. The pH effect was studied by mixing 0.8 g/L of the adsorbent with 20 ml of 50 mg/L of phosphate solution at different pH (2.0–11.0). As shown in Fig. S7, the optimum pH for removal of phosphate was 3.0 < pH < 6.0. According to the ionisation fraction and distribution diagram (Fig. S8), at pH ≤ 2, H_3PO_4 dominate the solution, while at 2.0 < pH < 7.2, $H_2PO_4^-$ controls the system. At 7.2 < pH < 12.3 and pH > 12.3, HPO_4^{2-} and $PO_4^{3-}$are the main species of phosphate in the solution, respectively.

The adsorption efficiency of these species is in order of $PO_4^{3-} > HPO_4^{2-} > H_2PO_4^- > H_3PO_4$. This explains why the removal rate of phosphate increased with pH increase. The equilibrium pH after phosphate adsorption decreased, compared with the initial pH, because of hydrogen ions released to the solution through ligand exchange; this is confirmed by the noticeable drop in pH > 7.0 after adsorption, Fig. 5a. The decline in adsorption (pH ≥ 7.0) is due to the presence of a high concentration of OH^-, which is competing with the phosphate ions.

At low pH, the MUC-PANI is easily protonated, enhancing the electrostatic force that favours phosphate adsorption. The surface electrostatic potential was assessed (Fig. 5b). The zeta potential was zero at pH 5.3, above which the z_t-potential was negative, causing electrostatic repulsion between the adsorbent and the adsorbate. However, even at pH 10, there was some adsorption of phosphate (35%). Because of this, and the fact that adsorption was less affected by

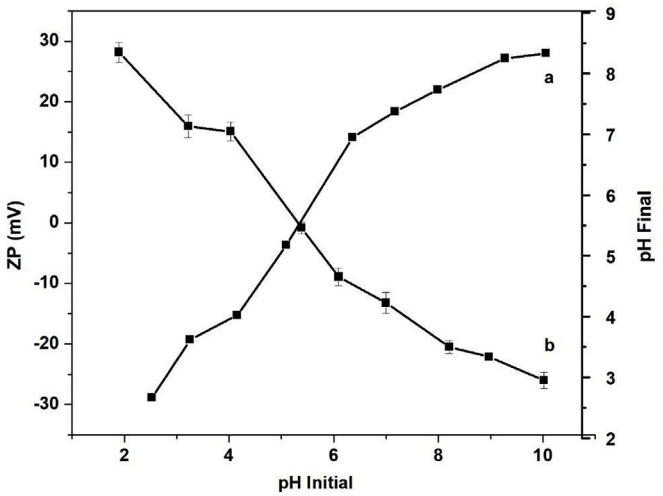

Fig. 5. pH change (a) before and after adsorption and (b) Zeta potential.

pH (2 < pH < 7), other mechanisms, rather than electrostatic force only, are suggested during the removal of phosphate.

3.3. Adsorption kinetics and rate-limiting step

The adsorption kinetics of phosphate onto the MUC-PANI are shown in Fig. S9a. Regardless of the initial adsorbate concentration, there was a rapid removal of phosphate within the first 15 min, owing to readily available sites on the MUC-PANI, as well as electrostatic attraction. Additionally, the highly interconnected pore structure accelerated the contact between the adsorbent and adsorbate. This expedited removal could help to reduce the reactor size during practical application. An analysis of 10 mg/L of the phosphate adsorption isotherm showed that at equilibrium, only 0.267 mg/L of the phosphate remained in solution, which is below the allowable 0.50–1.0 mg/L of effluent phosphate concentration.

To understand the adsorption mechanism of phosphate onto MUC-PANI, sorption kinetics were analysed using linear, pseudo first order (PFO), pseudo second order (PSO), and Elovich models, Eqs. S2-S4 (Blanchard et al., 1984; Lagergren, 1898; McLintock, 1967).

The kinetic model and error results are summarised in Table S4, Table S5, and Figs. S9b–S14.

According to the calculated correlation coefficient (R^2) and normalized standard deviation (NSD) values for linear models, adsorption kinetic data is best described with the PSO kinetic model. However, the linearization of the kinetics model distorts the distribution of error factor (Kajjumba et al., 2018b); therefore, non-linear models were used to predict the best kinetics. Analysis of all error functions for nonlinear adsorption kinetics (Table S5) indicated that the Elovich model provides the best fit for the adsorption of phosphate. Thus, the nature of adsorption on the heterogeneous surface of MUC-PANI is best described by chemisorption through inner-sphere complex formation. The valence forces are between the amine functional group on the polyaniline and phosphate, as shown in Eq.(3).

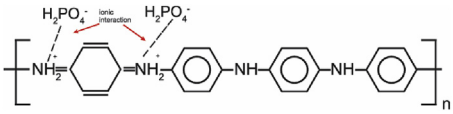

(3)

Neither PFO nor PSO kinetics can predict the diffusion mechanism—film diffusion and intra-particle diffusion that may control the adsorption process. To understand the rate-controlling step during adsorption, the intra-particle diffusion model was assessed using Eq. S(5).

Fig. S16 and Table S6 show the plots and results of the intra-particle diffusion model. The isotherm at 50 mg/L exhibits the largest initial boundary layer. The first sharp stage is due to the boundary layer diffusion of phosphate through the solution to the external surface of the MUC-PANI through a hydrodynamic boundary layer. The second section shows the gradual adsorption of the ions due to the abundant voids on the cross-linked MUC-PANI, with intra-particle diffusion being the rate-limiting step (Emik, 2014). The last section of the graph (after 120 min) shows equilibrium adsorption, where intra-particle diffusion becomes slow due to ligand exchange. To confirm whether intra-particle diffusion is the rate-limiting step during phosphate adsorption, a Boyd analysis was employed using Eq. (4) (Boyd et al., 1947):

$$F = 1 - \frac{6}{\pi^2}\sum_{1}^{\infty}\left(\frac{1}{n^2}\right)\exp(-n^2 B_t) \tag{4}$$

where F is the ratio of adsorbate adsorbed at time t to the amount adsorbed at an infinite time; n is the Freundlich constant, and B_t is a mathematical function of F. The values of F can be calculated using the expression below:

$$F = \frac{q_t}{q_\infty} \tag{5}$$

where q_∞ is the amount of phosphate adsorbed at the infinite time—48 h for this study. For simplicity, a Boyd equation can be rearranged in two forms as follows:

$$0 \le F \le 0.85:\ B_t = 2\pi - \frac{\pi^2 F}{3} - 2\pi\left(1 - \frac{\pi F}{3}\right)^{1/2} \tag{6}$$

and

$$0.86 \le F \le 1:\ B_t = -0.4977 - \ln(1 - F) \tag{7}$$

The values of F are calculated using Eq. (6), while B_t values are calculated based on Eqs. 7 and 11. The plot B_t vs time helps to predict the exact rate-limiting step during adsorption—either intra-particle or mass transport (Doğan and Aydın, 2014; Emik, 2014). When the plot of B_t vs t is equivalent to the graph y = bx, the governing step is intra-particle diffusion; otherwise, it is film diffusion. Albeit the plot of B_t vs t (Fig. S15) yielded a good correlation, the intercept is not zero, intra-particle diffusion is not the rate-limiting step. Therefore, different mechanisms controlled the adsorption of phosphate, but only one was rate limiting in a particular given time range.

3.4. Adsorption isotherms

The study of adsorption isotherms helps the understanding of the interface between solid and liquid phases at equilibrium, and the estimation of the adsorption capacity of an adsorbent. The two-parameter Langmuir and Freundlich isotherms were studied, while the Dubinin-Radushkevich (D-R) model was used to study the mean adsorption energy, Eqs. S6-S9 (Dubinin and Radushkevich, 1947; Freundlich, 1906; Langmuir, 1918).

Adsorption models of phosphate on the MUC-PANI were studied at 10.0, 25.0, and 40.0 °C, Fig. 6a–d. An increase in temperature increased adsorption capacity (Fig. 6a). Table 2 summarises the adsorption parameter of each model. The assessment of error parameters (Table S7) indicated that the Langmuir model (adsorption capacity = 147.1 mg/L at 298 K and pH 5.0) is the most appropriate for the fit of the equilibrium experimental data. Comparing the monolayer adsorption capacity (Table 3), the MUC-PANI exhibits a competitive capacity. Although the MUC-PANI did not show maximum q_m, its application in wastewater treatment offers a cost benefit, its skeleton is produced from cheap and readily available coal. In addition, with an influent concentration of 10 mg PO_4^{3-}/L, the MUC-PANI was able to remove over 97% of the phosphate. Such performance can supplement the biological processes to meet the stringent effluent standards.

To predict whether adsorption was a favoured mechanism during the removal of phosphate from the solution, the dimensionless seperation constant, R_L, was calculated using Eq. S(10). The R_L values between $0 < R_L < 1$ favour adsorption process (Emik, 2014). From Table 2, all the R_L values are below 1.0; thus, adsorption was favoured during the removal of phosphate. In addition, the values of 1/n are in the range of 0–1, which favours the adsorption mechanism (Emik, 2014; Kajjumba et al., 2018a).

To understand the adsorption mechanism, mean adsorption energy E, which explains the change in free energy when one mole of phosphate is adsorbed to the surface of the MUC-PANI, was assessed using Eq. S(11). When 1.0 < E < 8.0 kJ/mol, physical adsorption controls the adsorption, while when 8.0 < E < 16.0 kJ/mol, ion exchange dominates the adsorption process (Su et al., 2013). The values of E (Table 2) are below 8.0 kJ/mol at all temperatures, which indicates the ion exchange mechanism is not the only major force during the adsorption of phosphate.

3.5. Selectivity of MUC-PANI

Wastewater composition is complex with different ions and organic substances that can affect the removal of a target contaminant. The removal of phosphate by MUC-PANI was tested in a binary system containing Na_2CO_3, Na_2SO_4, and $NaNO_3$. At a low concentration of

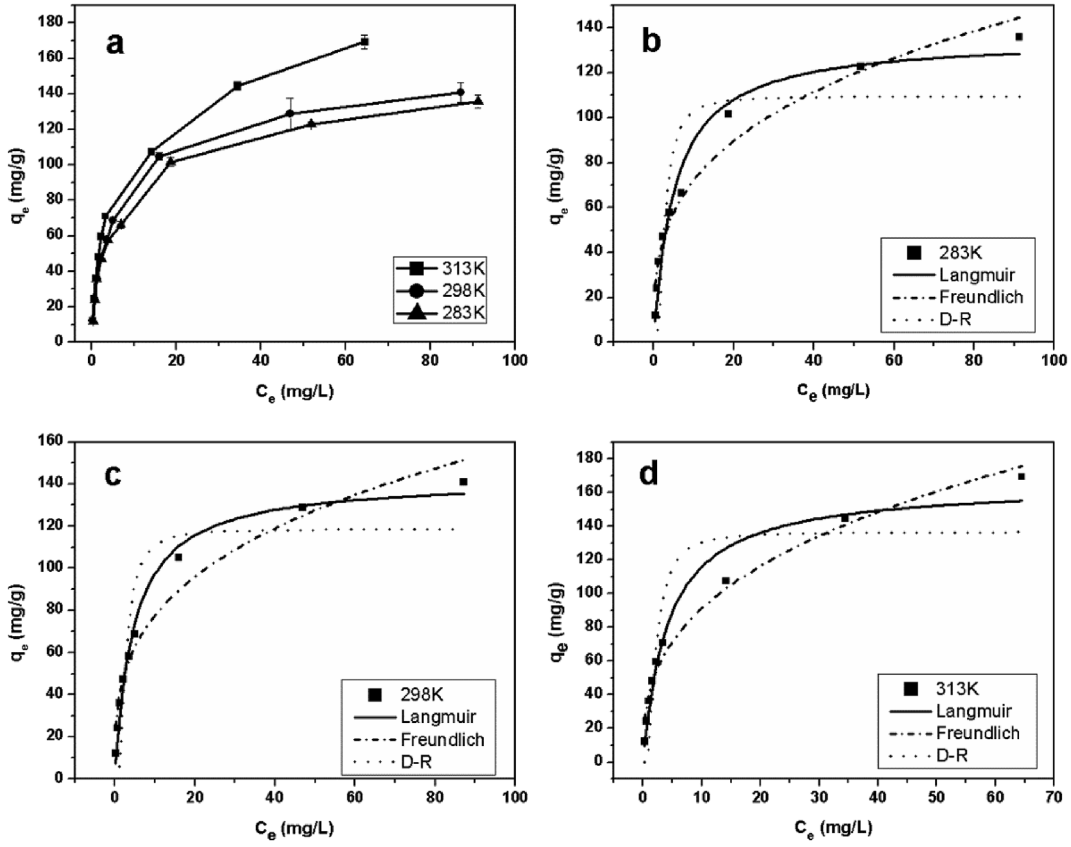

Fig. 6. Effect of (a) temperature on adsorption of phosphate (b)-(d) equilibrium isotherm at different temperatures; adsorbent dose = 0.8 g/L and pH 5.0.

Table 2
Adsorption isotherm coefficients.

Isotherm	Parameter	Temperature (K)		
		283.0	298.0	313.0
Langmuir	q_m (mg/g)	140.8	147.1	175.4
	b (L/mg)	0.190	0.219	0.210
	R_L	0.0256	0.0224	0.0232
	R^2	0.997	0.998	0.991
	NSD[a]	0.248	0.237	0.233
Freundlich	K_F ((mg/g)(L/mg)$^{1/n}$)	27.64	29.92	33.30
	1/n	0.404	0.404	0.439
	R^2	0.976	0.983	0.921
	NSD	0.474	0.361	0.465
D-R	$\beta_{DR} \times 10^{-9}$ (mol^2/J^2)	27.00	25.90	25.30
	q_{DR} (mg/g)	164.1	183.0	230.8
	E (KJ/mol)	4.303	4.394	4.446
	R^2	0.882	0.956	0.869
	NSD	1.638	0.265	1.229

[a] Normalized standard deviation.

Table 3
Comparison of phosphate adsorption capacity among different adsorbents.

Adsorbent	pH	Temp (K)	Dose (g/L)	q_m (mg/g)	Reference
Amorphous ZrO_2	6.2	298	0.1	99.00	Su et al., (2013)
Modified La_2O_3	5.6	298	0.5	58.70	Wu et al., (2019)
Modified bauxsol	4.2	325	0.5	192.9	Ye et al., (2016)
Bismuth-biochar	3.0	298	2.0	384.3	Zhu et al., (2016)
Iron-biochar	7.0	295	2.0	111.0	Yang et al., (2018)
Coal	5.0	298	0.8	46.34	This study
Modified coal	5.0	298	0.8	147.1	This study

competing ions, the removal of phosphate was less affected; however, the increase of carbonate concentration greatly affected the removal of phosphate (Fig. S19). Both nitrate and sulphate are strong nucleophiles; therefore, they are expected to compete favourably against phosphate during ligand exchange. However, neither of them form complex spheres with MUC-PANI; rather, they are good leaving groups, easily detaching from electrophiles (Schwarzenbach et al., 2003). Thus, phosphate ions can easily replace them on the amine functional group. Both carbonate and phosphate have the same nucleophilic strength. Thus, carbonate will compete for adsorption sites (through ligand exchange) with the same power as phosphate ions. Additionally, carbonate is not a good leaving group, as it forms multiple spheres with the MUC-PANI. This explains why the adsorption of phosphate decreased in the presence of carbonate ions.

3.6. Reusability

To test the reusability of MUC-PANI, the saturated/used adsorbent was mixed with 1M NaOH for approximately 24 h to desorb the phosphate and then regenerated with 2M HCl, dried at 110 °C, and reused. Fig. S20 shows the adsorbed fraction each time the MUC-PANI was reused. The adsorption capacity was over 90% for the first five cycles and dropped to 85% in the sixth cycle. This shows that MUC-PANI is a stable adsorbate. The decrease in the phosphate adsorption capacity is probably due to the diffusion and adsorption of some phosphate moieties into the deep pores or due to the formation of strong bonds with MUC-PANI.

4. Conclusion

This study modified unburnt coal, improving coal's adsorption capacity by a factor over three. Using coal as an adsorbent provides an environmentally friendly way of utilising coal. The removal of

phosphate by MUC-PANI is a complex mechanism, with an amine group on polyaniline playing a role in the removal of phosphate ions and/or ligand exchange. Between 3.0 < pH < 6.0, the adsorption of phosphate onto MUC-PANI was less affected. The rate-limiting step in the adsorption of phosphate is boundary layer diffusion. Phosphate adsorption was spontaneous during the first 15 min, and with an initial concentration of 10 mg/L, modified coal managed to remove over 97% of the phosphate. MUC-PANI has a competitive adsorption capacity compared to other adsorbents. At low concentrations, competing ions have less effect on the adsorption of phosphate.

Acknowledgement

This work was supported by the research fund of Istanbul University, Cerrahpaşa (Grant number 37685). Thanks to Murat Sirin, Betül Güleryüz, Elif Ağca, and Meagan Madariaga-Hopkins of the University of Nevada, Las Vegas, and Michael Kayemba of UZURI Advisory for data analysis, suggestions, and advice.

Appendix A. Supplementary data

Supplementary data to this article can be found online at https://doi.org/10.1016/j.jenvman.2019.06.088.

References

Blanchard, G., Maunaye, M., Martin, G., 1984. Removal of heavy metals from waters by means of natural zeolites. Water Res. 18, 1501–1507. https://doi.org/10.1016/0043-1354(84)90124-6.

Boyd, G.E., Adamson, A.W., Myers, L.S., 1947. The exchange adsorption of ions from aqueous solutions by organic zeolites. II. kinetics. J. Am. Chem. Soc. 69, 2836–2848. https://doi.org/10.1021/ja01203a066.

Cai, T., Park, S.Y., Li, Y., 2013. Nutrient recovery from wastewater streams by microalgae: status and prospects. Renew. Sustain. Energy Rev. 19, 360–369. https://doi.org/10.1016/j.rser.2012.11.030.

Chindaprasirt, P., Jaturapitakkul, C., Chalee, W., Rattanasak, U., 2009. Comparative study on the characteristics of fly ash and bottom ash geopolymers. Waste Manag. 29, 539–543. https://doi.org/10.1016/j.wasman.2008.06.023.

Darwish, M., Aris, A., Puteh, M.H., Jusoh, M.N.H., Abdul Kadir, A., 2017. Waste bones ash as an alternative source of P for struvite precipitation. J. Environ. Manag. 203, 861–866. https://doi.org/10.1016/j.jenvman.2016.02.033.

Doğan, V., Aydın, S., 2014. Vanadium(V) removal by adsorption onto activated carbon derived from starch industry waste sludge. Separ. Sci. Technol. 49, 1407–1415. https://doi.org/10.1080/01496395.2013.879312.

Dubinin, M.M., Radushkevich, L.V., 1947. The equation of the characteristic curve of activated charcoal. Proc. Acad. Sci. Phys. Chem. Sect. 1, 875.

Emik, S., 2014. Preparation and characterization of an IPN type chelating resin containing amino and carboxyl groups for removal of Cu(II) from aqueous solutions. React. Funct. Polym. 75, 63–74. https://doi.org/10.1016/j.reactfunctpolym.2013.12.006.

Földvári, M., 2011. Handbook of the Thermogravimetric System of Minerals and its Use in Geological Practice. Central European Geology. https://doi.org/10.1556/CEuGeol.56.2013.4.6.

Freundlich, H., 1906. Über die adsorption in lösungen. Z. Phys. Chem. 57, 385–471. https://doi.org/10.1515/zpch-1907-5723.

Gupta, T., 2018. Coal, the black carbon. Carbon N. Y. 139–173. https://doi.org/10.1007/978-3-319-66405-7_5.

Hallajiqomi, M., Eisazadeh, H., 2017. Adsorption of manganese ion using polyaniline and it's nanocomposite: kinetics and isotherm studies. J. Ind. Eng. Chem. 55, 191–197. https://doi.org/10.1016/j.jiec.2017.06.045.

Hao, R., Zhou, Y., Li, J., Wang, J., 2018. A 3DBER-S-EC process for simultaneous nitrogen and phosphorus removal from wastewater with low organic carbon content. J. Environ. Manag. 209, 57–64. https://doi.org/10.1016/j.jenvman.2017.12.018.

Kajjumba, G.W., Aydın, S., Güneysu, S., 2018a. Adsorption isotherms and kinetics of vanadium by shale and coal waste. Adsorpt. Sci. Technol. 36, 936–952. https://doi.org/10.1177/0263617417733586.

Kajjumba, G.W., Emik, S., Öngen, A., Özcan, H.K., Aydın, S., 2018b. Modelling of adsorption kinetic processes—errors, theory and application. In: Advanced Sorption Process Applications. IntechOpen, pp. 1–19. https://doi.org/10.5772/intechopen.80495.

Lagergren, S., 1898. About the theory of so-called adsorption of solid substance. Handlingar 24, 1–39.

Langmuir, I., 1918. The adsorption of gases on plane surfaces of glass, mica and platinum. J. Am. Chem. Soc. 40, 1361–1403. https://doi.org/10.1021/ja02242a004.

Li, C., Wan, J., Sun, H., Li, L., 2010. Investigation on the activation of coal gangue by a new compound method. J. Hazard Mater. 179, 515–520. https://doi.org/10.1016/j.jhazmat.2010.03.033.

Liu, H.B., Chen, T.H., Chang, D.Y., Chen, D., Liu, Y., He, H.P., Yuan, P., Frost, R., 2012. Nitrate reduction over nanoscale zero-valent iron prepared by hydrogen reduction of goethite. Mater. Chem. Phys. 133, 205–211. https://doi.org/10.1016/j.matchemphys.2012.01.008.

Lu, J. feng, Tsai, C.J., 2014. Hydrothermal phase transformation of hematite to magnetite. Nanoscale Res. Lett. 9, 1–8. https://doi.org/10.1186/1556-276X-9-230.

McLintock, I., 1967. The Elovich equation in chemisorption kinetics. Nature 216, 1204–1205. https://doi.org/10.1038/2161204a0.

Mo, J., Yang, Q., Zhang, N., Zhang, W., Zheng, Y., Zhang, Z., 2018. A review on agro-industrial waste (AIW) derived adsorbents for water and wastewater treatment. J. Environ. Manag. https://doi.org/10.1016/j.jenvman.2018.08.069.

Mthombeni, N.H., Mbakop, S., Ochieng, A., Onyango, M.S., 2016. Vanadium (V) adsorption isotherms and kinetics using polypyrrole coated magnetized natural zeolite. J. Taiwan Inst. Chem. Eng. 66, 172–180. https://doi.org/10.1016/j.jtice.2016.06.016.

Mujtaba, G., Rizwan, M., Lee, K., 2017. Removal of nutrients and COD from wastewater using symbiotic co-culture of bacterium Pseudomonas putida and immobilized microalga Chlorella vulgaris. J. Ind. Eng. Chem. 49, 145–151. https://doi.org/10.1016/j.jiec.2017.01.021.

Schwarzenbach, R.P., Gschwend, P.M., Imboden, D.M., 2003. Environmental Organic Chemestry. John Wiley & Sons, New Jersey. https://doi.org/10.1002/0471649643.

Socrates, G., 2004. Infrared and Raman Characteristic Group Frequencies. John Wiley and Sons. https://doi.org/10.1002/jrs.1238.

Su, Y., Cui, H., Li, Q., Gao, S., Shang, J.K., 2013. Strong adsorption of phosphate by amorphous zirconium oxide nanoparticles. Water Res. 47, 5018–5026. https://doi.org/10.1016/j.watres.2013.05.044.

Wang, S., Kong, L., Long, J., Su, M., Diao, Z., Chang, X., Chen, D., Song, G., Shih, K., 2018. Adsorption of phosphorus by calcium-flour biochar: isotherm, kinetic and transformation studies. Chemosphere 195, 666–672. https://doi.org/10.1016/j.chemosphere.2017.12.101.

Wu, Y., Li, X., Yang, Q., Wang, D., Xu, Q., Yao, F., Chen, F., Tao, Z., Huang, X., 2019. Hydrated lanthanum oxide-modified diatomite as highly efficient adsorbent for low-concentration phosphate removal from secondary effluents. J. Environ. Manag. 231, 370–379. https://doi.org/10.1016/j.jenvman.2018.10.059.

Xie, J., Wang, Z., Lu, S., Wu, D., Zhang, Z., Kong, H., 2014. Removal and recovery of phosphate from water by lanthanum hydroxide materials. Chem. Eng. J. 254, 163–170. https://doi.org/10.1016/j.cej.2014.05.113.

Yang, Q., Wang, X., Luo, W., Sun, J., Xu, Q., Chen, F., Zhao, J., Wang, S., Yao, F., Wang, D., Li, X., Zeng, G., 2018. Effectiveness and mechanisms of phosphate adsorption on iron-modified biochars derived from waste activated sludge. Bioresour. Technol. 247, 537–544. https://doi.org/10.1016/j.biortech.2017.09.136.

Yang, S.M., Chen, K.H., Yang, Y.F., 2005. Synthesis of polyaniline nanotubes in the channels of anodic alumina membrane. Synth. Met. 152, 65–68. https://doi.org/10.1016/j.synthmet.2005.07.142.

Ye, J., Cong, X., Zhang, P., Zeng, G., Hoffmann, E., Liu, Y., Wu, Y., Zhang, H., Fang, W., Hahn, H.H., 2016. Application of acid-activated Bauxsol for wastewater treatment with high phosphate concentration: characterization, adsorption optimization, and desorption behaviors. J. Environ. Manag. 167, 1–7. https://doi.org/10.1016/j.jenvman.2015.11.023.

Yuan, Y., Zhang, H., Pan, G., 2016. Flocculation of cyanobacterial cells using coal fly ash modified chitosan. Water Res. 97, 11–18. https://doi.org/10.1016/j.watres.2015.12.003.

Zhu, N., Yan, T., Qiao, J., Cao, H., 2016. Adsorption of arsenic, phosphorus and chromium by bismuth impregnated biochar: adsorption mechanism and depleted adsorbent utilization. Chemosphere 164, 32–40. https://doi.org/10.1016/j.chemosphere.2016.08.036.